NANO-MICRO LETTERS

Vol. 2, No. 2
60-67 (2010)

Reactive wetting behaviors of Sn/Cu systems: A molecular dynamics study

J. Y. Hsieh[1,2], J. L. Chen[3], C. Chen[4], H. C. Lin[5], S. S. Yang[5] and C. C. Hwang[5,*]

Influences of temperature and Sn-Cu droplet's composition on reactive wettings of Cu(100), Cu(110), and Cu(111) surfaces were analyzed, by using molecular dynamics (MD) calculations. As a result, the spreading on Cu(110)(Cu(100)) has the fastest (slowest) wetting kinetics. A higher temperature or a diluter Cu content in the Sn-Cu alloy droplet results in a higher wettability. Moreover, this work has addressed a theory for positioning the interface separating the liquidus and solidus alloys in the spreading film to confirm the hypothesis that the reactive wetting will come to the end when the interface saturates with the temperature-dependent solidus weight fraction of Cu.

Keywords: Wetting; Surface alloying; Molecular dynamics; Droplet

Citation: J. Y. Hsieh, J. L. Chen, C. Chen, H. C. Lin, S. S. Yang and C. C. Hwang, "Reactive wetting behaviors of Sn/Cu systems: A molecular dynamics study", Nano-Micro Lett. 2, 60-67 (2010). doi: 10.5101/nml.v2i2.p60-67

In recent years, lead free solders have been extensively proposed in utility of connecting devices to printed-circuit boards in microelectronic manufacturing because of legal, environmental and technological considerations [1]. In the soldering process, a metallurgical bond is formed between a molten solder and a metal surface. Therefore, the molten solder is required to properly spread, or wet, on the metal substrate for the formation of a proper metallic bond. The tendency for a metal to spread on a solid surface has been defined as the wettability [2]. In the case of inert liquid/solid combinations, the wettability can be evaluated by calculating the contact angle between the solder and the substrate via Young's equation, which gives the balance of the solid surface/gas, solid/liquid, and gas/liquid interfacial tensions at equilibrium. Nevertheless, Young's equation is less useful for the realistic soldering process, where the mechanical strength of a material joint depends significantly on the degree of reaction between the spreading solder and the solid substrate. Even so, a lower contact angle between the solder and the substrate in general corresponds to a lower surface interfacial energy and indicates a higher wettability. Particularly, surface alloying, which is resulted from the reaction between the solid surface and the liquid spreading on it, has been observed to improve wettability [3]. Therefore, reactive wettings are of particular interest in studies relevant to lead free soldering.

Acoff and coworkers[4,5], using sessile-droplet method, have reported the contact angle measurements of four lead free Sn-based alloys, namely Sn-3.5Ag, Sn-3.5Ag-4.8Bi, Sn-3.8Ag-0.7Cu, and Sn-0.7Cu (wt.%), on copper substrates. They found the Sn-3.5Ag-4.8Bi alloy exhibited the lowest contact angles indicating improved wettability with addition of bismuth and the contact angle decreased with increasing temperature, depending on the type of flux used in the sessile-droplet method. Amore et al. [6] have experimentally studied the surface tension and wetting behavior of molten Cu-Sn alloys on Ni substrate. They found their results of the surface tension of the Cu-Sn system are in good agreement with

[1]Department of Mechanical Engineering, Ming Hsin University of Science and Technology, Hsinchu 30401, Taiwan
[2]Institute of Precision Mechatronic Engineering, Ming Hsin University of Science and Technology, Hsinchu 30401, Taiwan
[3]Department of Mechanical Engineering, WuFeng Institute of Technology, Chiayi 621, Taiwan
[4]Department of Information Management, Meiho Institute of Technology, Pingtung 912, Taiwan
[5]Department of Engineering Science, National Cheng Kung University, Tainan 70101, Taiwan
[*]Corresponding author. Email: chchwang@mail.ncku.edu.tw

the works of Drath et al. [7] and Lee et al. [8] and concluded that the contact angle decreases with the increase of Sn-content for the Sn-rich Cu-Sn alloys. Other experimental studies on the wetting behavior of Sn-based lead free solders on metal substrate can also be found in refs [9-17].

Besides experimental methods, theoretical continuum models have also been proposed in studying the reactive wetting of solid surfaces [18-20]. However, continuum models inevitably make significant approximations because of lacking atomistic analyses of the wetting detail. Recently, molecular dynamics (MD) calculations have been implemented as atomistic simulations in researches of the reactive wetting since they are able to provide more robust constitution relations and more detailed surface transport mechanisms. Webb III and coworkers [21,22] studied the reactive wetting behaviors of liquid Pb and Ag on copper substrates, respectively. They demonstrated that in the liquid Pb wetting Cu(111) and Cu(100), a precursor film of atomic thickness spreads significantly faster on Cu(111) than on Cu(100) [21]. They also demonstrated that as liquid Ag spreads on Cu surface, wetting kinetics is enhanced by dissolution reactions [22].

In particular, knowledge of the reactive wetting of Sn/Cu systems is important for a lead free soldering process since Sn-Cu binary alloys can represent a basic subsystem of some Sn-based multi-element alloys proposed as alternative solder materials, such as Sn-Ag-Cu, Sn-Bi-Cu, and Sn-Ag-Cu-Sb, etc.. Relevant MD studies of the wetting of Cu substrate by pure Sn or Sn-Cu alloys, however, are rare. This work therefore attempts to perform MD calculations of the spreading of liquid Sn-Cu droplets, including a pure Sn droplet, on Cu crystals to study in detail the reactive wetting behaviors occurring within the liquid/solid system. This study is of two-fold interest. It is hoped to provide the physical insights of the wetting system and the necessary information required in a lead free soldering. The influences of the crystalline direction of the substrate surface, temperature, and the alloy droplet's composition on wetting kinetics will be examined, respectively. The wettings by pure Sn droplet will first be investigated. Webb III et al. [21,22] have hypothesized that the reactive wetting is dominantly driven by the dissolution of the substrate atom into the liquid until the liquid saturates in the substrate atom. This work will rephrase this hypothesis by assuming that the dominant force will stop driving the reactive wetting as long as an interface separating the liquidus and solidus alloys in the spreading film saturates with the temperature-dependent solidus weight fraction of the substrate atom and stops moving into the liquid. This hypothesis will be confirmed through establishing a theory for positioning the liquid/solid interface and determining its saturation with the solidus weight fraction of the substrate atom. The correctness of the hypothesis and the usability of the theory will be re-verified by the results of the remaining wettings, by the liquid Sn-Cu alloys.

This study simulated the reactive wettings of pure Sn and Sn-Cu alloy droplets on Cu(100), Cu(110), and Cu(111) surfaces, respectively. Positions and velocities of both the droplet and the substrate atoms were calculated as functions of time using MD methodology. The Cu-Cu, Cu-Sn, and Sn-Sn interactions are described by modified embedded atom method (MEAM) potentials [23]. All MEAM parameters used in the present calculations are from the report of Aguilar et al. [24]. In each of the present simulations, the spreading was considered as an isothermal process that both the droplet and the substrate were controlled at a common temperature that is higher than the solidifying point of the droplet. Figure 1 shows the configuration of the droplet wetting system considered in this work. Four droplets of pure Sn and Sn-Cu alloys, namely, Sn-10Cu, Sn-20Cu, and Sn-30Cu (wt%), respectively, were considered. Each of the droplets, with a diameter of about 5nm, comprised a fixed number of 3000 atoms. The solidifying temperatures, or, the liquidus temperature, of these droplets, evaluated in the present trial simulations, are about T_L^{Sn}=450K, T_L^{Sn10Cu}=600K, T_L^{Sn20Cu}=650K, and T_L^{Sn30Cu}=850K, respectively. The MEAM liquidus and solidus temperatures of the nanometer scale Sn-Cu binary considered here as functions of the weight fraction of Cu, W^{Cu}, are presented in Fig. 2. The droplet atoms were simulated as in free motion. Three FCC copper crystals were constructed as the substrates with the [100], [110], or [111] direction oriented along the z axis, respectively. The copper substrate was arranged in a finite slab with a lateral area of 106.50 Å × 106.50 Å and thickness of 9.03 Å for the Cu(100) substrate, with a lateral area of 162.05 Å × 162.05 Å and

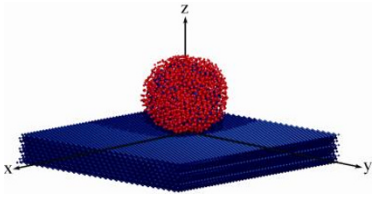

FIG. 1. Configuration of the wetting system. Droplets of pure Sn and Sn-10Cu, Sn-20Cu, and Sn-30Cu (wt%) were considered, respectively. Each droplet comprises 3000 atoms of Sn (red) and Cu (blue). Bottom of the substrate comprises two layers of rigid Cu atom. The origin of the coordinates is on the substrate surface. The center of the droplet was positioned on z axis and the bottom of the droplet was positioned about 3Å above the Cu surface when the system has been in equilibration.

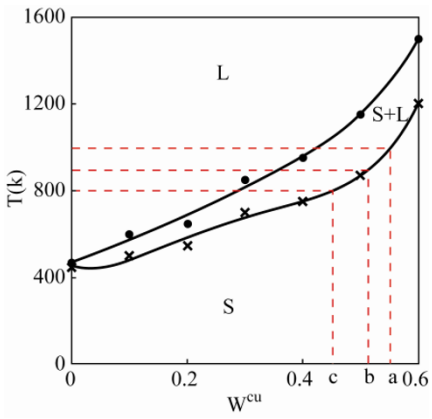

FIG. 2. Phase diagram of nanometer-scale Sn-Cu alloys. The range of weight fraction of Cu in the alloy considered in this diagram is between 0.0 and 0.6. The lower (upper) curve represents the solidus (liquidus) temperature as a function of the weight fraction of Cu.

thickness of 15.32 Å for the Cu(110) substrate, and with a lateral area of 131.83 Å × 131.83 Å and thickness of 16.63 Å for the Cu(111) substrate. The Cu(100), Cu(111), and Cu(110) substrates comprised 10800, 36608, and 28080 FCC copper atoms, respectively. The bottom of the substrate was two layers of rigid atoms and the remaining part of the substrate consists of free motion atoms. In the present MD simulations, periodic boundary conditions were applied in the directions in the plane of the free surfaces (x and y).

A constant time increment Δt=2 fs for integrating the equations of motion for all non-rigid atoms was employed in the present computations. Each MD simulation performed herein comprised the stage of the equilibration of the droplet/substrate system and the stage of spreading. The equilibration stage consumed a computation time of 20 ps, which is sufficiently long for the relaxation of both the droplet and the substrate. After this stage, the bottom of the droplet was positioned about 3 Å above the substrate surface such that the effect of the long-range attractive force between the drop and substrate can be avoided. The initial positions of the pure Sn droplet atoms were randomized and the substrate atoms were arranged in accordance with their crystalline structures, respectively. The arrangement of randomized positions of the Sn droplet is rational because the droplet is in liquid phase, as can also be seen in ref. [25], in which MEAM molecular dynamics was implemented to study the physical mixture of nano-Sn and nano-Ag particles. In this work, the influence of droplet composition was studied using binary Sn-Cu liquids. To do so, Cu atoms were randomly substituted for Sn atoms in the liquid to achieve the desired weight fraction of Cu, W_0^{Cu}. In this work, the alloy droplets with W_0^{Cu}=0.1, 0.2, and 0.3 were used in the wetting simulations, respectively. For all the cases studied here, the initial velocities of all atoms in the spreading system were randomized according to the specific temperature using numbers uniformly distributed in an interval. The spreading stage then started when both the droplet and substrate have been relaxed to their equilibrium atomic configurations. The spreading stage lasted for 300 ps, which is long enough for the spreading process to become steady. In all the present MD simulations, the temperatures of the whole spreading system were held at a desired value using the rescaling method [26,27]. The leap-frog algorithm was implemented to derive new position and velocity vectors of the droplet and the substrate atoms from the corresponding data obtained in the previous step. The motion of each atom in the system was governed by Newton's law of motion in which the resulting force acting on the atom was deduced from energy potential relevant to the interactions with the neighboring atoms within a cut-off radius.

In the studies of dissolutive wettings of Cu substrates by liquid Pb and Ag, Webb III *et al.* [21,22] pointed out that dissolution of the substrate atom into the liquid drop, over the incorporation of the liquid atom into the solid substrate, is the dominant driving force of the reactive spreading until the liquid saturates in the substrate material. Like the Pb/Cu and Ag/Cu systems, for the present cases, a pure Sn or a Sn-Cu binary droplet placed on pure Cu will dissolve Cu into the droplet as it spreads. Accompanied with the dissolution of Cu, Sn will also be incorporated into the Cu lattice. However, attentions will be paid only on regimes where dissolution of solid into the liquid is dominant, because incorporation of Sn into the Cu lattice to form an equilibrium solid solution involves solid state diffusion that will consume a time far beyond the capability of atomistic simulations. In the present cases, since Sn droplet spreads on Cu substrate more quickly than Ag droplet does, the saturation of the liquid Sn droplet in Cu will be completed in a rather short time and therefore can be observed more sufficiently. In fact, all wettings simulated in this work have already come to the end before the simulation time of 300 ps. Figure 3 shows the cross-section snapshots from simulations when the wettings by the pure Sn droplet at 1000K have taken place for 300 ps on the three Cu substrates, respectively. During the spreading progress, surface alloying reaction on the substrate surfaces can be observed through the occurrence of the dissolution of Cu atoms into the liquid Sn droplet and the incorporation of Sn atoms into the Cu crystal. To quantify the wetting kinetics of the Sn droplet on Cu substrates, the temporal evolutions of the radial extension of the droplet R(t) on the various Cu substrates and at 800K and 1000K are demonstrated in Fig. 4, respectively. (The result for 900K is in between those for 800K and 1000K, but it is not

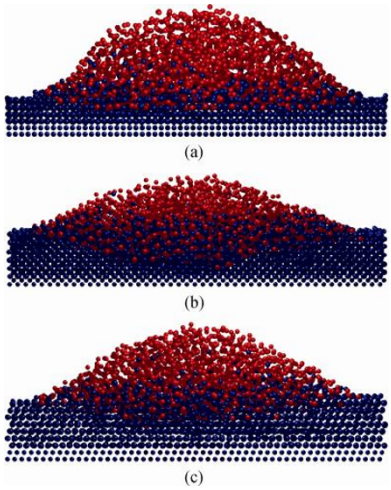

FIG. 3. Cross-section snapshots from simulations when the wettings by the pure Sn droplet at 1000K have taken place for 300 ps on (a) Cu(100); (b) Cu(110); and (c) Cu(111) planes, respectively. Surface alloying is observed through the interchange of Sn (red) and Cu(blue) atoms across the substrate surface.

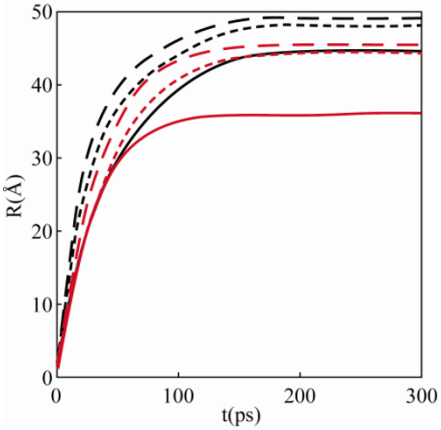

FIG. 4. Variations of radius of the spreading film, R(t), for the Sn droplets wetting on Cu(100) (solid curves), Cu(110) (long dashed curves), and Cu(111) (short dashed curves) at 800K (red curves) and 1000K (black curves), respectively.

shown here.) In the present analysis, the radial extension R(t) is derived from the contact area of the nearest slab of the drop atoms above the substrate surface. As shown in Fig. 4, at a common temperature, the fastest wetting kinetics of the Sn droplet is on Cu(110), while the slowest one is on Cu(100) and in between is on Cu(111), but the radial extensions tend to become steady at approximately equal times. The difference of wetting kinetics is simply attributed to the distinct planar crystalline structures on these surface planes. On the (110) plane, the FCC copper atoms are less closely packed than those packed on the (111) and (100) planes, so Cu atoms on this plane dissolute into the liquid drop and bind to Sn atoms to form a surface alloy in a larger area at a time than those on the other planes do. The quicker (slower) radial extension on (110) ((100)) plane, however, gives rise to a lesser (denser) density of Cu in the alloy film, so Cu atoms from deeper (shallower) planes of the Cu crystal will melt into the droplet to complete the spreading at the specific temperature. As a result, the wettings on these planes tend to become steady at equal times. The R(t) curves in Fig. 4 also indicate that in the early stage of the reactive wetting, all the film radii grow with $t^{1/2}$ and they have become steady quite early before 300 ps. Furthermore, the R(t) curves in Fig. 4 demonstrate a natural phenomenon that a higher temperature (meaning that the droplet has higher kinetic energy) leads to a quicker radius growth. However, on a specific surface plane, the radius growth tends to become steady at an earlier time instant when wetting is performed at a lower temperature, reflecting the fact that the droplet saturates in a less Cu content for a lower temperature. In addition, as the radial extension comes to the end, a larger final radius also implies a smaller final contact angle. In this study, the final contact angle was simply approximated by calculating the formula θ_f=arctan(h/R), where h represents the height of the final film. The final contact angles of all Sn droplet wetting simulations performed in this work are listed in the first data row in Table 1. As shown, among all of the present simulations, the highest wettability is achieved when Sn wets the Cu(110) surface at 1000K, since the final contact angle in this case is the smallest.

The results shown in Figs. 4 lead to the conclusion that the 300 ps simulation time used in all the simulations performed herein is in fact sufficiently long, and the ending of all the wettings is thus designated to be at 300 ps. The Sn droplet wets the various Cu substrates with different speeds, but all the wettings should cease when the droplet saturates in Cu atoms; the latter phenomenon, however, should depend only on the temperature. To discuss the driving mechanism of the reactive

Table 1. The final contact angles obtained in all the simulations performed in this work.

Temperature / Surface / Droplet	1000K			900K			800K		
	Cu(100)	Cu(111)	Cu(110)	Cu(100)	Cu(111)	Cu(110)	Cu(100)	Cu(111)	Cu(110)
100wt%Sn	28.56	25.77	20.15	34.07	29.25	25.92	40.95	34.45	31.57
Sn-10wt%Cu	29.61	27.48	24.41	34.10	32.40	28.28	41.80	35.20	34.9
Sn-20wt%Cu	32.01	29.52	24.88	35.83	32.26	29.83	42.53	37.76	35.11
Sn-30wt%Cu	32.63	29.55	25.80	36.82	32.38	30.5	NA	NA	NA

wetting in more details, the density profiles for Cu and Sn in the wettings of the various surfaces by the pure Sn at 1000 K as functions of z after 300 ps are demonstrated in Fig. 5, as an example for depiction. The density function was calculated as an average over a circular region with radius 25 Å in x-y plane and with its center positioned at z axis. As demonstrated in Fig. 5, the crossover of the density profiles for both Cu and Sn around the substrate surface (z=0) clearly displays the inter-diffusion of these atoms occurring near the substrate surface during the wetting process. The domain where such crossover occurs thus is termed the inter-diffusion zone, or surface alloy zone. The density profiles for Cu in Fig. 5 show that, while Cu atoms of deeper planes remain intact, as reflected by the same density peaks on these planes, the upper planes of Cu in the crystal have decreased peak peaks of density, indicating that more Cu atoms on upper planes in part have melted into the liquid film. The reactive wetting of Cu(110) ((100)) achieves the thickest (thinnest) surface alloy layer. As shown, eleven (110) planes, five (111) planes, and only two (100) plans have decreased density peaks for Cu in the substrates, respectively. In the same time, Sn atoms have diffused into the Cu lattice; Sn can even be seen in the eighth (110) plane but only in the second (100) plane under the substrate surface. Several coexisting density peaks for Cu and Sn in the spreading film (z>0) also are found in the zone nearest to the substrate surface, implying the planar crystalline structure of the Sn-Cu alloy in this zone. In the spreading film, owing to the dissolution of Cu into the liquid, if Cu increases to some limit, depending on the specific temperature of the wetting system, then the Sn-Cu alloy will first become liquidus, i.e., the binary alloy is in liquid and solid phases simultaneously. Further increase of Cu content will cause the Sn-Cu binary composition to reach another limit, so the specific system temperature will become the solidus temperature of the alloy at which the Sn-Cu alloy will be solidified to its crystalline structure. The descending density peaks for Cu along z axis in Fig. 5 reveal that the solidification of the Sn-Cu alloy in the droplet is localized in the zone nearest to the substrate surface and the liquidus binary alloy is located above this zone. In this work, the theoretical boarder separating the solidus and liquidus binary alloys is defined as the liquid/solid interface of the surface alloy. During the wetting process, the zone of crystalline binary alloy will extend up into the spreading droplet, or, the liquid/solid interface will move upwards. Specifically, Webb III *et al.* have hypothesized that the reactive wetting of metallic droplet and substrate will proceed until the liquid droplet saturates in substrate atoms. In this work, the hypothesis is expressed as the reactive wetting proceeds until the liquid/solid interface stops moving upwards, while saturating with the solidus weight fraction of the substrate atom. However, a sharp liquid/solid interface in fact is not distinguishable; the density profiles in Fig. 5 cannot help identifying the liquid/solid interface precisely. This work thus presents a simple theory for positioning the theoretical liquid/solid interface, which should utilize the temperature-dependent solidus weight fraction of Cu in the Sn-Cu binary system, $W_S^{Cu}(T)$, as shown in Fig. 2. To determine the position of the liquid/solid interface, density peaks for Cu in the inter-diffusion zone are first used for curve-fitting a continuous density function, viz., $\rho_{Cu}(z)$. Then the liquid/solid interface of the surface alloy is defined to be located at $z=z_{int}$ such that the second order differential derivative of the density function with respect to z vanishes, i.e., $d^2\rho_{Cu}(z_{int})/dz^2=0$, because the density for Cu at that point will be steady (i.e. time-independent) whereas the interface stops moving upwards, if the continuum model of mass diffusion is applied. Meanwhile, for each of the planes of atoms in the inter-diffusion zone, the density peaks for Cu and Sn of the plane are used for calculating the average weight fraction of Cu in the Sn-Cu binary system on the plane. At $z=z_{int}$, the weight fraction of Cu in the binary alloy, denoted by $W^{Cu}(z_{int})$, can be simply determined as the linear interpolation of the values at the two neighboring points that z_{int} is in between. The diagrammatic depiction of the determinations of z_{int} and $W^{Cu}(z_{int})$ in the wetting of Cu(100) by Sn droplet at 1000K can be found in Fig.6, only for instance. During the spreading process, the position of the liquid/solid interface z_{int} will move upwards and the weight fraction $W^{Cu}(z_{int})$ will increase with time as Cu atoms from the crystal keep melting into the droplet. The hypothesis presented here is that at a specific temperature T, the reactive wetting of Cu substrate by Sn or Sn-Cu alloys will come to the end when the liquid/solid interface stops at the final position $z_{int,f}$ and saturates with Cu, i.e., $W^{Cu}(z_{int,f})= W_S^{Cu}(T)$. Diagrammatic depiction of the movement of the liquid/solid interface for the wetting on Cu(100) plane performed at 1000K is demonstrated in the inset of Fig. 6. The black solid curves in Fig. 4 and the inset of Fig. 6 exhibit that both the growth of the spreading film's radius and the movement of the liquid/solid interface become steady at the same time. The weight fraction $W_S^{Cu}(T)$ is dependent only on temperature and independent of the crystalline direction of the Cu substrate surface that the droplet wets. The results of all Sn wettings listed in the first data row of Table 2 have verified the correctness of the present

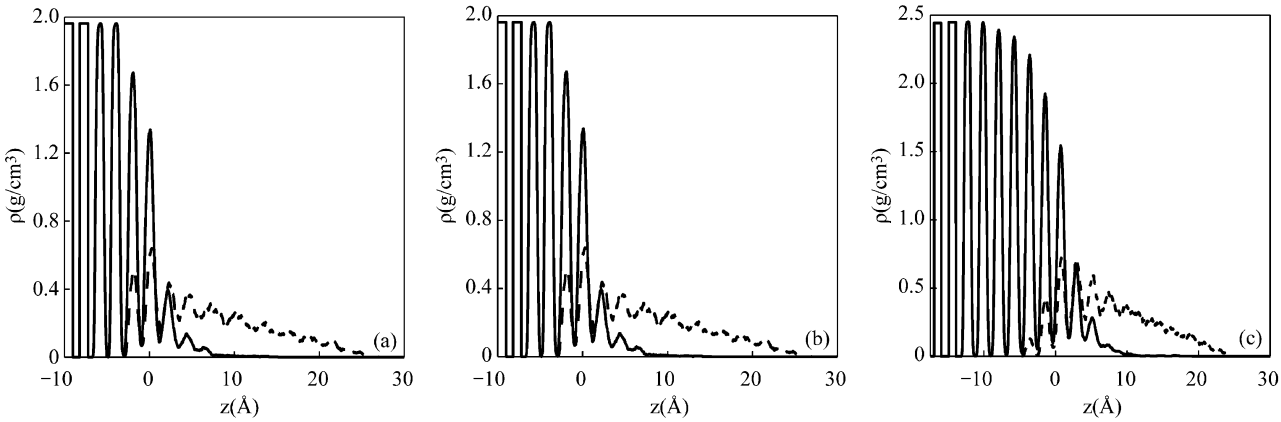

FIG. 5. Density profiles for Cu(black) and Sn(blue) as functions of z at 300 ps in the wettings by liquid Sn on (a) Cu(100); (b) Cu(110); and (c) Cu(111) planes performed at 1000K, respectively.

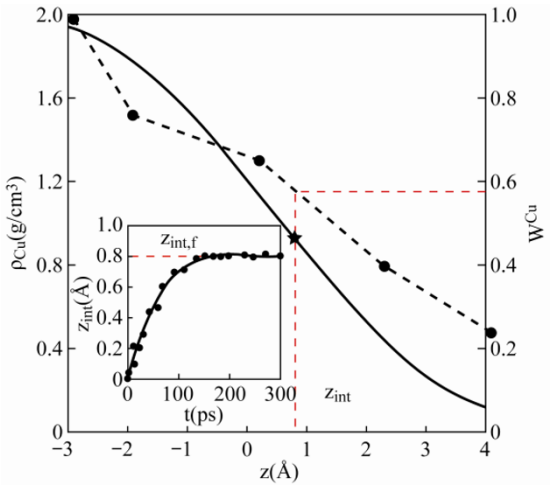

FIG. 6. Diagrammatic depiction for determining position of the theoretical liquid/solid interface, z_{int}, and the weight fraction of Cu at that position, $W^{Cu}(z_{int})$. First establish the curve-fitting density function $\rho_{Cu}(z)$, using data of the density peak for Cu in the inter-diffusion zone, and then determine the position of the interface by letting $d^2\rho_{Cu}(z)/dz^2=0$. Finally, compute the corresponding weight fraction of Cu, using data of density peak for Cu in the inter-diffusion zone, and determine the weight fraction of Cu at the interface by linearly interpolating the values at the neighboring points that the interface is in between. The inset shows the variation of z_{int} with time for the Sn wetting on Cu(100) at 1000K, for a depiction example.

hypothesis and the usability of the present theory. The results listed in Table 2 reveal that, when performed at a specific temperature T, wettings on the various substrates considered herein have approximately a common $W^{Cu}(z_{int,f})$, which is very close to $W_S^{Cu}(T)$. Effects of the crystalline direction of Cu surface only lead to different wetting kinetics and different positions of the liquid/solid interface. At a common temperature, the wetting on (110) plane gives the upmost final position of the liquid/solid interface and that on (100) plane, the lowest position, simply because the former has the fastest spreading kinetics and the latter, the slowest.

The density profiles for Cu and Sn mentioned above are averages over the circular region with radius 25 Å in x-y plane and thus are simply expressed as z-dependent functions, and so is the z-dependent weight fraction of Cu. Nevertheless, the distribution of the weight fraction of Cu in the inter-diffusion zone in fact is more likely two-dimensional (axially symmetric). Displayed in Fig. 7 are, in color scale, the distributions of W^{Cu} on several planes perpendicular to z axis for the wettings of Cu(100) performed at 1000K; as shown in the figure, the distributions are approximately axially symmetric. The planes considered in Fig. 7 are the nearest layers to the substrate surface and are positioned at which the density peaks for Cu shown in Fig. 5 occur, including the first two layers above (at $z=z_1$ and $z=z_2$) and under the substrate surface (at $z=z_{-1}$ and $z=z_{-2}$), respectively. Figure 7 clearly shows that, on the layers under the substrate surface, weight fraction of Cu in the region nearer to z axis is smaller, indicating that majorities of the Cu and Sn atoms that have melted into the liquid and incorporated into the crystal, respectively, come from this region. In contrast to these layers, on the layers above the substrate surface diluter content of Cu is also observed in the region nearer to z axis. In this work, on a plane the region around z axis, where the weight fraction of Cu is relatively small, is called the core zone of the plane. As shown in Fig. 7, both liquid and solid alloys co-exist on the layer positioned at z_2, which is above the theoretical liquid/solid interface, while only solid alloys exist on the layer positioned at z_1, which instead is under the liquid/solid interface. Interestingly, on the plane z_2, the liquid alloys (with smaller W^{Cu}) in the core zone are surrounded by the solid alloys (with larger W^{Cu}). The distributions of weight fraction of Cu demonstrated in Fig. 7 depict that when substrate Cu atoms, especially those in the core zone, followed by the Cu atoms from lower layers, face the liquid they will melt into it. The Cu atoms in the liquid then will diffuse outwards to the edge of the spreading film and finally, together with Sn atoms, adhere to the underlying solid, causing larger W^{Cu} in region farther from the core zone. Near the end of the spreading, only Cu atoms in the core zone, if still unsaturated, will melt into the liquid. The present evidence shows the liquid/solid interface is theoretically positioned in

Table 2. The final positions of liquid/solid interface, $z_{int,f}$ (Å), and the corresponding weight fractions of Cu at the interface, $W^{Cu}(z_{int,f})$, in all the wettings simulated in this work.

Temperature	1000K			900K			800K		
Surface / Droplet	Cu(100)	Cu(111)	Cu(110)	Cu(100)	Cu(111)	Cu(110)	Cu(100)	Cu(111)	Cu(110)
100wt%Sn	0.80 (0.567)	1.25 (0.567)	1.30 (0.558)	1.20 (0.519)	1.45 (0.515)	1.88 (0.512)	1.42 (0.450)	1.88 (0.450)	1.90 (0.451)
Sn-10wt%Cu	0.83 (0.568)	1.27 (0.562)	1.35 (0.562)	1.45 (0.520)	1.60 (0.510)	1.92 (0.509)	1.70 (0.452)	2.05 (0.452)	2.15 (0.450)
Sn-20wt%Cu	0.87 (0.566)	1.71 (0.564)	1.90 (0.560)	1.50 (0.520)	1.90 (0.516)	1.95 (0.508)	1.78 (0.456)	2.08 (0.458)	2.20 (0.453)
Sn-30wt%Cu	1.20 (0.572)	1.80 (0.565)	1.97 (0.566)	1.80 (0.520)	2.03 (0.518)	2.10 (0.514)	NA	NA	NA
$W^{Cu}(z_{int,f})$ Average ± deviation		0.56 ± 0.003			0.515 ± 0.004			0.452 ± 0.002	

Data shown here exhibits that $W^{Cu}(z_{int,f})$ depends only on temperature. Average and deviation of the temperature-dependent $W^{Cu}(z_{int,f})$ are 0.564±0.003, 0.515±0.004, and 0.452±0.002 for 1000K, 900K, and 800K, respectively. These data are very close to the temperature-dependent solidus weight fractions W_S^{Cu}(1000K)=0.562, W_S^{Cu}(900K)=0.518, and W_S^{Cu}(800K)=0.457, respectively.

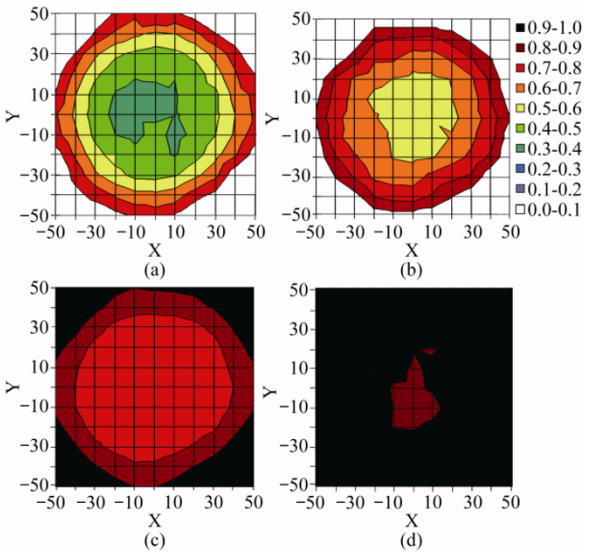

FIG. 7. Cross-section snapshots at 300 ps showing color scaled distributions of weight fraction of Cu on planes perpendicular to z axis for the wettings of Cu(100) at 1000K. The planes considered here are at (a) z_2=1.965 Å; (b) z_1=0.621 Å; (c) z_{-1}=-2.103 Å; and (d) z_{-2}=-4.051 Å, respectively. Inside the broken circle in each diagram is the area over which the densities of Cu and Sn are averaged.

between the planes z_1 and z_2. Under the interface, the core zone of plane z_1 is in solid phase and above it, the core zone of plane z_2 is still in liquid phase. Obviously, the melting of Cu into the liquid stops when the core zone of the theoretical interface is saturated with the solidus weight fraction W_S^{Cu}.

Figure 8 shows the influence of droplet composition on the radial extension R(t); a richer Cu content in the alloy droplet results in a slower wetting kinetics, the same trend as in the case of wetting by Cu-Ag alloys [22]. However, radial extensions in the wettings by the alloys in different compositions require approximately equal time to become steady. This is simply due to that, during the reactive wetting by a richer (diluter) Cu content droplet, fewer (more) Cu atoms are required to melt into the droplet to cause its saturation with Cu. Similar to the wettings by Sn, the time required for the radius growth in the Sn-Cu wettings to become steady is almost independent of the crystalline direction of the substrate surface. The final contact angles of the wettings of the various Sn-Cu droplets performed at the various temperatures considered in this work are also listed in Table 1. This table depicts that the contact angle decreases with the decrease of Cu content for the Sn-rich Cu-Sn alloys, qualitatively consistent with the macroscopic observations of Amore et al. [6]. The hypothesis and theory described above can also be applied to the wettings by Sn-Cu alloy droplets. In the cases of the Sn-Cu droplet wettings, the final positions of the liquid/solid interface $z_{int,f}$ and the corresponding values of $W^{Cu}(z_{int,f})$ were obtained following the same procedure mentioned above. The results are listed in Table 2. Again, the hypothesis presented in this work is verified by the fact that, at a common temperature T, the weight fractions of Cu at the liquid/ solid interfaces $W^{Cu}(z_{int,f})$ have approximately the same value of $W_S^{Cu}(T)$ for the wettings of the various alloy droplets. However, a richer Cu content in the binary alloy droplet results in an upper position of the liquid/solid interface.

In this work, a total of 36 MD calculations for simulating

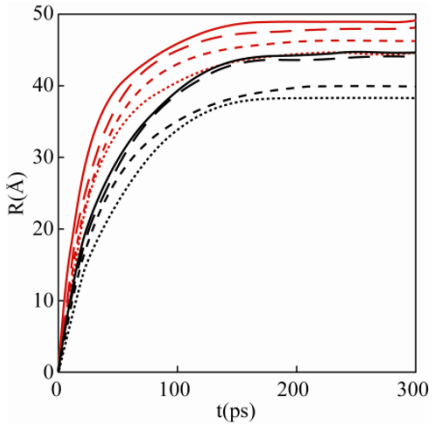

FIG. 8. Variations of radius, R(t), for the spreading films of Sn (solid curves), Sn-10Cu (long dashed curves), Sn-20Cu (short dashed curves), and Sn-30Cu (dotted curves) on Cu(100) (black curves) and Cu(110) (red curves), respectively. Presented here are the results from the wettings performed at 1000K. The influence of the droplet's alloy composition at other temperatures is similar to what is shown here.

reactive wettings of Sn/Cu systems have been performed. Reactive wettings of Cu(100), Cu(110), and Cu(111) substrates by pure Sn and Sn-10Cu, Sn-20Cu, and Sn-30Cu(wt%) alloy droplets at the temperatures of 800K, 900K, and 1000K were considered, respectively. The simulation results show that the spreading of Cu(110)(Cu(100)) substrate has the fastest (slowest) wetting kinetics and the highest (lowest) final position of the theoretical liquid/solid interface separating the liquidus and solidus Sn-Cu alloys in the surface alloy film. Wettings performed at a higher temperature also have faster kinetics but require longer times to become steady. A higher temperature will lower the position of the liquid/solid interface in the surface alloy. Meanwhile, the influence of the droplet's alloy composition is that a richer Cu content causes the alloy droplet to wet the substrates with a slower kinetics and a higher position of the liquid/solid interface. This work considered the regime where the dissolution of the substrate Cu into the liquid dominates the reactive wetting. A hypothesis that the reactive wetting will come to the end as the theoretical liquid/solid interface saturates with the temperature-dependent solidus weight fraction of Cu and stops moving into the droplet has been confirmed through a theory successfully developed in this work for positioning the liquid/solid interface in the spreading film. However, the realistic distribution of the weight fraction of Cu in the surface alloy is axially symmetric. In the region farther from z axis richer contents of Cu are observed both in the alloys above and under the substrate surface, reflecting less amount of Cu in the crystal have melted into the liquid droplet and the Cu atom that have melted into the droplet tend to diffuse to the edge of the liquid film. In the zone of coexisting liquid and solid alloys, the liquid alloy is surrounded by the solid alloy. Summarized, this work has presented detail knowledge of the reactive wetting of Sn/Cu systems, which is necessarily required in relevant lead free soldering processes.

Received 11 March 2010; accepted 1 April 2010; published online 22 April 2010.

References

1. M. Abtew and G. Selvaduray, Mater. Sci. Eng. 27, 95 (2000). doi:10.1016/S0927-796X(00)00010-3
2. K. J. R. Wassink and M. M. F. Verguld, Manufacturing Techniques for Surface Mounted Assemblies GB-Port Erin, British Isles: Electrochemical Publications Ltd., 1995.
3. C. Iwamoto and S. Tanaka, Acta. Mater. 41, 749 (2002). doi:10.1016/S1359-6454(01)00388-3
4. M. F. Arenas, M. He and V. L. Acoff, J. Electron. Mater. 35, 1530 (2006). doi:10.1007/s11664-006-0144-7
5. M. F. Arenas and V. L. Acoff, J. Electron. Mater. 33, 1452 (2004). doi:10.1007/s11664-004-0086-x
6. S. Amore, E. Ricci, T. Lanata and R. Novakovic, J. Alloys Compd. 452, 161 (2008). doi:10.1016/j.jallcom.2007.01.178
7. G. Drath, S. Sauerwald and Z.Anorg, Chemistry 162, 301 (1927).
8. J. Lee, W. Shimoda and T. Tanaka, Mater. Trans. 45, 2864 (2004). doi:10.2320/matertrans.45.2864
9. H. K. Kim and K. N. Tuv, Phys. Rev. B 53, 16027 (1996). doi:10.1103/PhysRevB.53.16027
10. K. Suganuma, K. Niihara, T. Shoutoku and Y. Nakamura, J. Mater. Res. 13, 2859 (1998). doi:10.1557/JMR.1998.0391
11. J. W. Jang, P. G. Kim and K. N. Tu, J. Mater. Res. 14, 3895 (1999). doi:10.1557/JMR.1999.0527
12. T. Takemoto and M. Miyazaki, Mater. Trans. 42, 745 (2001). doi:10.2320/matertrans.42.745
13. C. B. Lee, S. B. Jung, Y. E. Shin and C. C. Shur, Mater. Trans. 42, 751 (2001). doi:10.2320/matertrans.42.751
14. T. Takao and H. Hasegawa, Mater. Trans. 45, 747 (2004). doi:10.2320/matertrans.45.747
15. H. Wang, F. Wang, F. Gao, X. Ma and Y. Qian, J. Alloys Compd. 433, 302 (2007). doi:10.1016/j.jallcom.2006.06.076
16. M. J. Rizvi, C. Bailey, Y. C. Chan and H. Lu, J. Alloys Compd. 438, 116 (2007). doi:10.1016/j.jallcom.2006.08.048
17. H. Ma, H. Xie and L. Wang, J. Mater. Sci. Technol. 23, 81 (2007). doi:10.1179/174328407X176839
18. F. Yost, E. O'Tool, Acta. Mater. 46, 5143 (1998). doi:10.1016/S1359-6454(98)00146-3
19. J. A. Warren, W. J. Boettinger and A. R. Roosen, Acta. Mater. 46, 3247 (1998). doi:10.1016/S1359-6454(97)00487-4
20. A. Mortensen, B. Drevet and N. Eustathopoulos, Scr. Mater. 45, 953 (2001). doi:10.1016/S1359-6462(01)01117-4
21. E. B. Webb III, G. S. Grest and D. R. Heine, Phys. Rev. Lett. 91, 236102 (2003). doi:10.1103/PhysRevLett.91.236102
22. E. B. Webb III, G. S. Grest, D. R. Heine and J. J. Hoyt, Acta. Mater. 53, 3163 (2005). doi:10.1016/j.actamat.2005.03.021
23. M. I. Baskes, Phys. Rev. B 46, 2727 (1992). doi:10.1103/PhysRevB.46.2727
24. J. F. Aguilar, R. Ravelo and M. I. Baskes, Modelling Simul. Mater. Sci. Eng. 8, 335 (2000). doi:10.1088/0965-0393/8/3/313
25. H. Dong, L. Fan, K. Moon, C. P. Wong and M. I. Baskes, Modelling Simul. Mater. Sci. Eng. 13, 1279 (2005). doi:10.1088/0965-0393/13/8/006.
26. D. C. Rapaport, The Art of Molecular Dynamics Simulation, Cambridge University Press, London, 1997.
27. D. Frenkel and B. Smit, Understanding Molecular Simulation, Academic, San Diego, 1996.